

PACS numbers: 68.37.Hk, 68.43.Mn, 68.43.Nr, 75.50.Tt, 78.67.Rb, 81.07.Wx, 81.16.Be

Nickel–Yttrium Ferrite Nanopowders for Solving Environmental Problems

B. K. Ostafiychuk, V. S. Bushkova, N. I. Riznychuk, R. S. Solovei,
and I. P. Yaremiy

*Vasyl Stefanyk Precarpathian National University,
57, Shevchenko Str.,
UA-76025 Ivano-Frankivsk, Ukraine*

Among the family of spinel ferrites, nickel ferrite NiFe_2O_4 obtained by ceramic technology was widely studied due to its tremendous properties such as high electromagnetic performance, excellent chemical stability and mechanical hardness, and moderate saturation magnetization, making it as a good contender for the application as soft magnets and low-loss materials at high frequencies. The structure, mechanical, magnetic, electrical, and dielectric properties of nickel ferrite are dependent on several factors including the method of fabrication, sintering time and temperature, chemical composition, type and amount of dopant, grain structure. The sol–gel processing with autocombustion (SGA) technique was used for the synthesis of $\text{NiY}_x\text{Fe}_{2-x}\text{O}_4$ ($x = 0.0, 0.1, 0.2, 0.3, 0.4, 0.5$) ferrite nanoparticles. The mixed solution was dried at temperature around 403 K. During evaporation, the solution becomes viscous and finally formed as a xerogel. At further elevation of temperature, the organic constituents are decomposed with the generation of gases such as CO_2 , N_2 and H_2O ; therefore, the xerogel automatically ignited. The autocombustion was completed within a few seconds, yielding the nanopowders of nickel–yttrium ferrites. The XRD results confirm single-phase formation of the as-prepared NiFe_2O_4 sample. The powders substituted with Y^{3+} ions, except the spinel-type phase, contain additional $\alpha\text{-Fe}_2\text{O}_3$ and Y_2O_3 phases too. The powder sizes decrease from 43 nm to 17 nm with increase in amount of Y^{3+} ions. The EDX results confirm the presence of Ni, Fe, Y, and O elements in Ni–Y-ferrite powders. The infrared (IR) spectra were recorded at the room temperature in the range from 400 cm^{-1} to 4000 cm^{-1} ; they confirm the spinel structure. As found, the adsorption capacity of Ni–Y ferrite increases, while the substitutions with Y^{3+} ions increase. The adsorption process increases with increasing pH, has a maximum at $\text{pH} = 7$, and depends on the dye type.

Серед феритів зі структурою шпінелі властивості фериту ніклю NiFe_2O_4 , одержаного за керамічною технологією, є широко вивчені, оскільки він

має високу електромагнетну продуктивність, відмінні хемічну стабільність і механічну твердість, а також помірну намагнетованість насити, що робить його хорошим претендентом для застосування як м'якого магнетного матеріалу з низькими втратами на високих частотах. Структура, механічні, магнетні, електричні та діелектричні властивості фериту нікелю залежать від декількох чинників, включаючи спосіб приготування, час і температуру спікання, хемічний склад, тип і кількість легувальної домішки та зернисту структуру. Наночастинки феритів $\text{NiY}_x\text{Fe}_{2-x}\text{O}_4$ ($x = 0,0, 0,1, 0,2, 0,3, 0,4, 0,5$) були синтезовані за допомогою методи золь-гель за участю автогоріння (ЗГА). Одержаний розчин було висушено за температури близько 403 К. Під час випарювання розчин поступово ставав в'язким, в результаті чого сформувався ксерогель. За подальшого підвищення температури органічні складові розклагалися з утворенням газів, таких як CO_2 , N_2 і H_2O . Процес автоматичного згорання ксерогелю завершився протягом декількох секунд, що привело до утворення нанопорошків нікель-ітрійових феритів. Результати X-променевого дослідження підтверджують утворення однофазного зразка NiFe_2O_4 . Заміщені йонами Y^{3+} порошки, крім фази шпінелі, містять також додаткові фази $\alpha\text{-Fe}_2\text{O}_3$ і Y_2O_3 . Із збільшенням кількості йонів Y^{3+} розміри порошків феритів зменшуються від 43 нм до 17 нм. Результати EDX-аналізи підтверджують наявність елементів Ni, Fe, Y і O у порошках Ni-Y-феритів. Інфрачервоні спектри реєстрували за кімнатної температури в діапазоні від 400 см^{-1} до 4000 см^{-1} ; вони також підтверджують, що порошки мають структуру шпінелі. Встановлено, що адсорбційна здатність Ni-Y-феритів зростає, в той час як заміщення йонами Y^{3+} збільшується. Процес адсорбції зростає зі збільшенням рівня рН, є максимальним при рН = 7 і залежить від типу барвника.

Среди ферритов со структурой шпинели свойства феррита никеля NiFe_2O_4 , полученного по керамической технологии, широко изучены, так как он обладает высокой электромагнитной проводимостью, отличной химической стабильностью и механической твердостью, а также умеренной намагниченностью насыщения, что делает его хорошим претендентом для применения как мягкого магнитного материала с низкими потерями на высоких частотах. Структура, механические, магнитные, электрические и диэлектрические свойства феррита никеля зависят от нескольких факторов, включая способ приготовления, время и температуру спекания, химический состав, тип и количество легирующей примеси, зернистую структуру. Наночастицы ферритов $\text{NiY}_x\text{Fe}_{2-x}\text{O}_4$ ($x = 0,0, 0,1, 0,2, 0,3, 0,4, 0,5$) были синтезированы с помощью метода золь-гель с участием автосгорания (ЗГА). Полученный раствор был высушен при температуре около 403 К. Во время выпаривания раствор постепенно становился вязким, в результате чего сформировался ксерогель. При дальнейшем повышении температуры органические составляющие разложились с образованием газов, таких как CO_2 , N_2 и H_2O . Процесс автоматического сгорания ксерогелей завершился в течение нескольких секунд, что привело к образованию нанопорошков никель-иттриевых ферритов. Результаты рентгеновских исследований подтверждают образование однофазного образца NiFe_2O_4 . Замещенные ионами Y^{3+} порошки, кроме фазы шпинели, содержат дополнительные фазы $\alpha\text{-Fe}_2\text{O}_3$ и Y_2O_3 . С

увеличением количества ионов Y^{3+} размеры порошков ферритов уменьшаются от 43 нм до 17 нм. Результаты EDX-анализа подтверждают наличие элементов Ni, Fe, Y и O в порошках Ni–Y-ферритов. Инфракрасные спектры регистрировали при комнатной температуре в диапазоне от 400 см^{-1} до 4000 см^{-1} ; они также подтверждают, что порошки имеют структуру шпинели. Установлено, что адсорбционная способность Ni–Y-ферритов растёт, в то время как замещение ионами Y^{3+} увеличивается. Процесс адсорбции возрастает с увеличением уровня pH, является максимальным при $\text{pH} = 7$ и зависит от типа красителя.

Key words: ferrite, nanopowder, EDX analysis, IR spectroscopy, adsorption capacity.

Ключові слова: ферит, нанопорошок, EDX-аналіза, ІЧ-спектроскопія, вбирна здатність.

Ключевые слова: феррит, нанопорошок, EDX-анализ, ИК-спектроскопия, адсорбционная способность.

(Received 26 March, 2019; after revision, 31 March, 2019)

1. INTRODUCTION

The development of society is inextricably linked with the increase in volumes of toxic waste that the environment cannot reprocess. With wastewater from industrial enterprises, a significant amount of pollution enters in the environment that is environmentally inappropriate. The most dangerous pollutants are highly toxic heavy metal ions. In recent years, the adsorption process in conjunction with magnetic separation technology is widely used to remove dyes from sewage. In this case, nanosize magnetic materials are used for production magnetic nanosorbents [1].

Recently, several works [2, 3] have been published, in which the removal of dyes from sewage by means of spinel oxide materials is investigated. The ferrites with spinel structure are widely used as refractory materials, catalysts or carriers of catalysts, humidity sensors, microwave dielectric and ceramic capacitors [4, 5].

The nanopowder spinel oxide materials have high mechanical strength, good thermal stability, and firmness to chemical influences. They are also durable and inexpensive. Nanosize spinel magnetic particles are effective adsorbents in connection with their large surface area. Since, ferrites with a spinel structure exhibit good magnetic properties their unique advantage is the easy separation under the action of an external magnetic field. This leads to their widespread use, in particular for the separation of dyes.

The nickel ferrite NiFe_2O_4 is a soft magnetic material, which

crystallizes to the cubic mixed spinel structure with space group $Fd3m$ [6]. This compound is represented as $(\text{Ni}_{\delta}^{2+}\text{Fe}_{1-\delta}^{3+})[\text{Ni}_{1-\delta}^{2+}\text{Fe}_{1+\delta}^{3+}]\text{O}_4$, where cations inside the round and square brackets occupy A -sites and B -sites, respectively, and δ (degree of inversion) depends on thermal history and preparation condition. Its magnetic ordering temperature is of about 580°C [7] that is far above the room temperature. It exhibits moderate saturation magnetization, excellent chemical, thermal and structural stability at room temperature [8]. Hence, this material is a promising candidate for a wide variety of technological applications at room temperature such as drug delivery, magnetic sensors, actuators, memory and high frequency devices [9].

The magnetic behaviour in this material is governed by the spin coupling of the unpaired $3d$ electrons of the Ni^{2+} and Fe^{3+} cations presented at the A and B sites. Among these superexchange interactions, the interaction between moments at the A and B sites is the strongest one, which mainly controls the magnetic behaviour of the NiFe_2O_4 .

The physical properties of nickel ferrite nanoparticles depend upon its size and composition. The size of the particle can be controlled by restricting particle rate of the nucleation and its subsequent growth with introducing a large strain at the lattice site by incorporating suitable substituent element [10]. Rare earth elements (Y^{3+} , La^{3+} , Gd^{3+} , Sm^{3+} , etc.) have larger ionic size than that of the Ni and Fe ions. Substituting of rare earth cations at the Ni and/or Fe sites will create a large strain at the lattice site, which may restrict the rate of the nucleation of the particle and its subsequent growth.

The synthesis of rare earth cations substituted spinel ferrite by solid state route suffers from drawbacks like phase segregation of metal monoxides, hematite and orthoferrites even for very low concentration of rare earth cations substitution [11]. However, the synthesis of rare-earth substituted nanocrystalline spinel ferrites in single-phase form is possible using chemical route despite having big difference in ionic radius of rare-earth cations and Ni^{2+} or Fe^{3+} cations.

Hence, the present report is aimed to synthesis the nickel ferrites substituted by Y^{3+} cations using SGA-technique and investigates their structural, chemical, and adsorption properties.

2. EXPERIMENTS

Yttrium (Y^{3+}) substituted nickel ferrite compound with empirical formula $\text{NiY}_x\text{Fe}_{2-x}\text{O}_4$ ($x = 0.0, 0.1, 0.2, 0.3, 0.4, 0.5$) has been synthesized by SGA-technique. The nickel nitrate ($\text{Ni}(\text{NO}_3)_2 \cdot 6\text{H}_2\text{O}$), iron nitrate ($\text{Fe}(\text{NO}_3)_3 \cdot 9\text{H}_2\text{O}$), yttrium nitrate ($\text{Y}(\text{NO}_3)_3 \cdot 6\text{H}_2\text{O}$), and citric

acid ($C_6H_8O_7 \cdot H_2O$) supplied with 99.9% purity were used as starting materials.

The x-ray diffraction patterns were recorded at room temperature on DRON 7 x-ray diffractometer using CuK_α radiation. The morphology of nickel-manganese ferrite powders were observed by scanning electron microscopy (SEM) with a Hitachi S-4700 electron microscope operating at 20.0 kV. The atomic weight composition (%) of the constituent elements in the as-prepared samples was carried out by energy dispersive x-ray spectroscopy (EDX) performed on the EXPERT 3L atomic composition analyser.

Infrared spectra (IR) for the gel precursor and the SGA powder were recorded on a NICOLETIS 10 spectrophotometer in the range 400–4000 cm^{-1} by the KBr pellet method. Processing of the results was carried out in software OMNIC 8.1. The surface absorbance capability of $NiY_xFe_{2-x}O_4$ nanoparticles were determined using Brunauer-Emmett-Teller (BET) surface-area technique using N_2 adsorption/desorption studies. The specific surface area of the samples was calculated for a linear graph of dependence $1/[W(P_0/P) - 1]$ on P/P_0 in the area of adsorption isotherm in limited range of $P/P_0 = 0.05-0.35$.

3. RESULTS AND DISCUSSION

3.1. X-Ray Diffraction (XRD)

The XRD pattern recorded at room temperature for the samples $NiY_{0.1}Fe_{1.9}O_4$, $NiY_{0.2}Fe_{1.8}O_4$, $NiY_{0.3}Fe_{1.7}O_4$, $NiY_{0.4}Fe_{1.6}O_4$ and $NiY_{0.5}Fe_{1.5}O_4$ are shown in Fig. 1. The diffraction patterns consist of well-resolved peaks, which have been indexed to $Fd3m$ space group in cubic symmetry. The peaks can be indexed to (111), (220), (311), (222), (400), (422), (511) and (440) planes.

For $NiFe_2O_4$, it has not been observed any additional peaks [4]. The powder doped with Y^{3+} ions, except the spinel-type phase, contains additional phases of $\alpha-Fe_2O_3$ and Y_2O_3 . The x-ray diffraction patterns of $NiY_{0.5}Fe_{1.5}O_4$ powder confirm the presence of an additional phase of $\alpha-Fe_2O_3$ because these powder has peaks at 24.50° , 33.44° , 36.30° , 41.62° , 49.72° , 54.33° , 57.46° , 62.05° , 64.06° from crystallographic planes (012), (104), (110), (113), (024), (116), (018), (214), (300). For $NiY_{0.1}Fe_{1.9}O_4$ powder, corresponding peaks are observed at 24.29° , 33.29° , 35.90° , 41.16° , 49.64° , 54.25° , 57.17° , 61.83° , 63.85° . Thus, for $NiY_xFe_{2-x}O_4$ spinel with height x , there is a slight shift of Bragg's peaks to the right, indicating a change in the lattice parameter a . It is also worth noting that the increase in the content of Y^{3+} ions in ferrites increases the amount

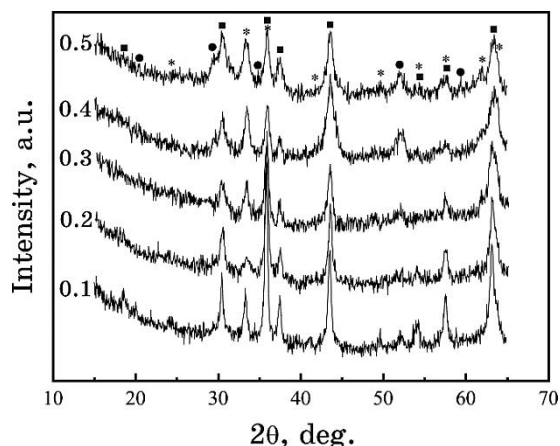


Fig. 1. X-ray spectra of $\text{NiY}_x\text{Fe}_{2-x}\text{O}_4$ powders, where ■ corresponds to the spinel phase; * and ● correspond to $\alpha\text{-Fe}_2\text{O}_3$ and Y_2O_3 , respectively.

of $\alpha\text{-Fe}_2\text{O}_3$ and Y_2O_3 oxides.

In addition, one could observe closely from the above XRD patterns that intensity of the diffraction peaks decreases, and the peaks become broader by substitution of Y^{3+} ions in place of Fe ions. For the clarity of the apparent peak broadening and decrease in peak intensity, the zoom plot of intense peak (311) has been depicted in Fig. 2. It indicates a related decrease of the crystallite size and/or presence of lattice strain.

The average size of coherent scattering regions (CSR) in the powders of nickel–yttrium ferrites was found from the most intense peak (311) of spinel phase using the Scherrer relationship:

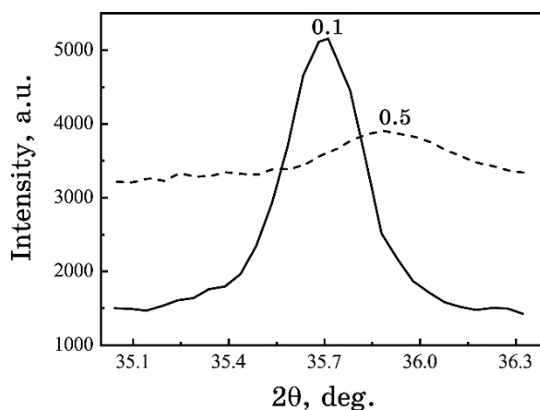


Fig. 2. The comparison of the (311) peak for the $\text{NiY}_x\text{Fe}_{2-x}\text{O}_4$ samples with $x = 0.0$ and 0.5 .

$$\langle D \rangle = \frac{0.9\lambda}{\beta \cos \theta}, \quad (1)$$

where β is the effective half-width of the diffraction peak for x-rays with wavelength λ at an angle 2θ . The average size of CSRs of powders was in the range 17–43 nm.

The lattice parameters for the $\text{NiY}_x\text{Fe}_{2-x}\text{O}_4$ samples ($x = 0.0, 0.1, 0.2, 0.3, 0.4, 0.5$) were obtained from x-ray data analysis. It has been observed that the lattice constant decreases slightly with substitution of Fe^{3+} by Y^{3+} ions. The radius of the octahedral site is larger than the tetrahedral site in the spinel lattice. The ionic radius of the Y^{3+} ion (0.091 nm) is large enough for octahedral site. One can assume that small amount of Y^{3+} cations can be substituted for Fe^{3+} cations, which enter into the octahedral sites by redistribution of cations between the tetrahedral and octahedral sites to minimize the free energy of the system. It appears that there is a partial migration of Ni^{2+} ions (0.069 nm) from *B* sites to *A* ones accompanied by an opposite transfer of equivalent number of Fe^{3+} ions (0.0645 nm) from *A* sites to *B* ones in order to relax the strain at the octahedral sites.

The decreasing of lattice constant is also evident from Fig. 2, because the Bragg peak position for $\text{NiY}_{0.5}\text{Fe}_{1.5}\text{O}_4$ is shifted a little to the right of the $\text{NiY}_{0.1}\text{Fe}_{1.9}\text{O}_4$ ferrite samples. The increase in diffraction angle means a decrease in the lattice constant for the Y^{3+} substituted samples.

3.2. Morphology Study

SEM micrographs of as-prepared ferrite powders are given in Fig.

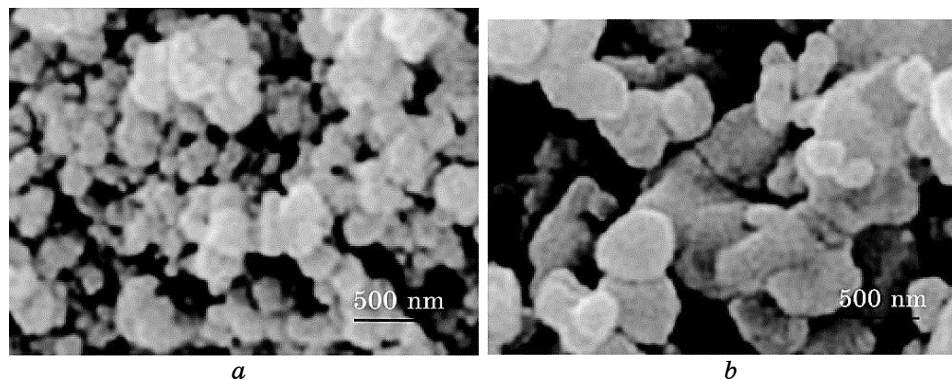


Fig. 3. SEM micrograph of Ni-Y ferrites: *a*— $\text{NiY}_{0.1}\text{Fe}_{1.9}\text{O}_4$; *b*— $\text{NiY}_{0.5}\text{Fe}_{1.5}\text{O}_4$.

3. Figure 3, *a, b* shows the surface of the $\text{NiY}_{0.1}\text{Fe}_{1.9}\text{O}_4$ and $\text{NiY}_{0.5}\text{Fe}_{1.5}\text{O}_4$ samples. Both samples have been characterized by SEM microscopy to study their morphology, size, shape and agglomeration. The SEM image of $\text{NiY}_{0.5}\text{Fe}_{1.5}\text{O}_4$ (Fig. 3, *b*) reveals that the morphology of the particles was dispersed uniformly with a wider range of particle sizes, whereas grain growth was apparent in $\text{NiY}_{0.1}\text{Fe}_{1.9}\text{O}_4$ (Fig. 3, *a*). The particles are agglomerated due to interaction between magnetic nanoparticles. This is a typical characteristic feature of spinel ferrite nanoparticles synthesized by sol-gel method [12, 13].

3.3. Elemental Analysis

A typical EDX spectrum of the as-prepared NiFe_2O_4 and $\text{NiY}_{0.5}\text{Fe}_{1.5}\text{O}_4$ samples are depicted in Fig. 4. As it was expected, the Fe^{3+} concentration is the highest one for $x = 0.0$. The percentage of Fe^{3+} decreases as the Y^{3+} substitution increases. The contents of the metals in the resulting spinel ferrites are close to the theoretical

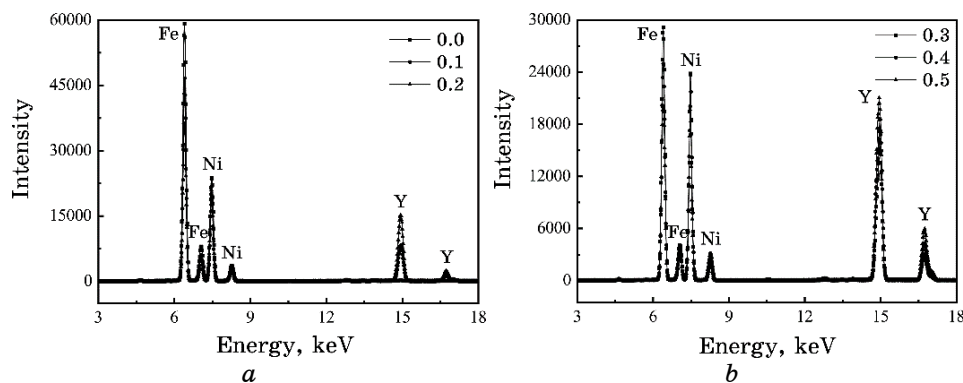


Fig. 4. EDX spectra of $\text{NiY}_x\text{Fe}_{2-x}\text{O}_4$ samples: *a*— $0.0 \leq x \leq 0.2$; *b*— $0.3 \leq x \leq 0.5$.

TABLE 1. The chemical formula of the Ni–Y ferrites.

x	Theoretical	Experimental
0.0	NiFe_2O_4	$\text{Ni}_{1.03}\text{Fe}_{1.91}\text{O}_{4.06}$
0.1	$\text{NiY}_{0.1}\text{Fe}_{1.9}\text{O}_4$	$\text{Ni}_{1.02}\text{Y}_{0.10}\text{Fe}_{1.86}\text{O}_{4.04}$
0.2	$\text{NiY}_{0.2}\text{Fe}_{1.8}\text{O}_4$	$\text{Ni}_{1.02}\text{Y}_{0.20}\text{Fe}_{1.73}\text{O}_{4.05}$
0.3	$\text{NiY}_{0.3}\text{Fe}_{1.7}\text{O}_4$	$\text{Ni}_{1.03}\text{Y}_{0.28}\text{Fe}_{1.65}\text{O}_{4.03}$
0.4	$\text{NiY}_{0.4}\text{Fe}_{1.6}\text{O}_4$	$\text{Ni}_{1.02}\text{Y}_{0.40}\text{Fe}_{1.56}\text{O}_{4.02}$
0.5	$\text{NiY}_{0.5}\text{Fe}_{1.5}\text{O}_4$	$\text{Ni}_{1.02}\text{Y}_{0.50}\text{Fe}_{1.42}\text{O}_{4.06}$

TABLE 2. Atomic weight composition of the constituent elements of the $\text{NiY}_x\text{Fe}_{2-x}\text{O}_4$.

x	Element	Theoretical		Experimental	
		wt. %	at. %	wt. %	at. %
0.0	O	27.31	57.14	28.03	58.05
	Fe	47.65	28.57	45.91	27.24
	Ni	25.04	14.29	26.06	14.71
0.1	O	26.93	57.14	27.32	57.67
	Fe	44.64	27.14	43.46	26.28
	Ni	24.69	14.29	25.33	14.57
	Y	3.74	1.43	3.89	1.48
0.2	O	26.56	57.14	27.07	57.80
	Fe	41.71	25.71	40.43	24.73
	Ni	24.35	14.29	25.15	14.64
	Y	7.38	2.86	7.35	2.83
0.3	O	26.20	57.14	26.61	57.61
	Fe	38.86	24.29	38.03	23.59
	Ni	24.02	14.29	25.01	14.76
	Y	10.92	4.28	10.35	4.03
0.4	O	25.85	57.14	26.02	57.39
	Fe	36.09	22.86	35.34	22.34
	Ni	23.70	14.29	24.15	14.52
	Y	14.36	5.71	14.49	5.75
0.5	O	25.51	57.14	26.19	58.00
	Fe	33.38	21.43	31.94	20.27
	Ni	23.39	14.29	24.20	14.61
	Y	17.72	7.14	17.87	7.12

values as shown by EDX analysis. The theoretical and experimental chemical formulas of the Ni–Y ferrites are listed in Table 1.

The theoretically expected stoichiometric molar amounts of various elements of the samples are comparable with the values obtained by the EDX analysis (Table 2). For example, for nickel ferrite, the atomic composition ratios of Ni, Fe and O were found to be 14.71%, 27.24% and 58.05%, respectively. For $\text{NiY}_{0.5}\text{Fe}_{1.5}\text{O}_4$ ferrite, the atomic composition ratios of Ni, Y, Fe and O were found to be 14.61%, 7.12%, 20.27% and 58.00%, respectively, which match well the amount of Ni, Y and Fe used in the respective precursors.

3.4. IR Spectroscopy

The IR spectra of the ferrite materials are an important tool to describe the various ordering problems, also, in the investigation of the structural properties of the mixed ferrites. They give infor-

mation not only about the positions of the ions in the spinel lattice crystal, but also about their vibrational mode. The vibrational spectra can be indicated to the valance state of the ions and their occupation in the spinel lattice crystal. Application of the IR spectroscopy to the ferrite materials is to detect the completion of the solid-state reaction, the cations distribution, and the deformation of spinel structure [14].

The IR spectral adsorption bands mainly appear due to the vibrations of the oxygen ions with the cations corresponding to various frequencies in the unit cell. In a certain mixed spinel ferrite materials, as the concentration of the divalent metal ions increasing, it gives rise to a structural change or cation distribution in the spinel crystal lattice without affecting the spinel ferrite structure. The structural changes brought about by the metal ions that are either lighter or heavier than divalent ions in the ferrites strongly influence the lattice vibrations. The vibrational frequency depends on the cation mass, the cation oxygen distance and the bonding force.

Figure 5 shows the IR spectra of the nickel ferrite. The dried gel shows the characteristic bands at about 1300, 1600 and 3250 cm^{-1} corresponding to NO_3^- ion, carboxyl $-\text{COO}-$ group and the O-H group, respectively. The existence of the characteristic bands of NO_3^- indicated that the NO_3^- as a group exists in the structure of citrate gel during the gelation of the mixed solution formed from nitrates and citric acid. The band at about 3050 cm^{-1} is assigned to the stretching vibrations of the O-H groups of hydrogen bonding at short distances [15].

The spectrum of the as-prepared powder gives a significant band at 560 cm^{-1} , which is the characteristic band of ferrite. The absence of spectroscopic band corresponding to the carboxyl group and nitrate ion at 1600 and 1300 cm^{-1} , respectively, suggests that these

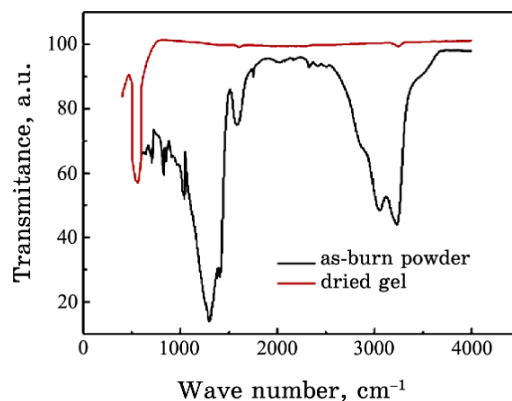


Fig. 5. IR-spectra of the dried gel and as-prepared NiFe_2O_4 powder.

groups take part in the reaction during the combustion process. Therefore, the combustion can be considered as a thermally induced anionic redox reaction of the gel wherein the citrate ion acts as a reductant and the nitrate ion acts as an oxidant. This autocombustion reaction forms the spinel structure of ferrite with the evolution of heat.

3.5. BET Surface Area

The specific surface area values were obtained by BET isotherms with N_2 adsorption. The surface area of $NiY_{0.5}Fe_{1.5}O_4$ ($31.8 \text{ m}^2/\text{g}$) was found to be higher than that of $NiFe_2O_4$ ($7.2 \text{ m}^2/\text{g}$). High surface area of $NiY_{0.5}Fe_{1.5}O_4$ is due to the smaller particle size of the sample, which is confirmed by XRD. Thus, the surface area increases with addition of Y^{3+} ions' content in the Ni–Y ferrites due to decreases of particles' size. This dependence of the specific surface area on the particles' size has been already observed in Ref. [16]. From this, it is expected that the high surface area of $NiY_{0.5}Fe_{1.5}O_4$ could enhance the catalytic and adsorption properties, than that of $NiFe_2O_4$.

Figure 6 shows nanopores' size distributions obtained from the adsorption branch of nitrogen sorption isotherms, using Barrett–Joyner–Halenda (BJH) analysis. All samples show relatively narrow pore size distribution with pore size varied from 2 to 5 nm, thus, in the mesoporous range (2–50 nm) according to IUPAC classification. The experimental result showed that nanopores with a radius of about 3 nm exercise the main contribution to the total pore volume for sample with $x = 0.5$ and, for sample $NiFe_2O_4$, 4 nm.

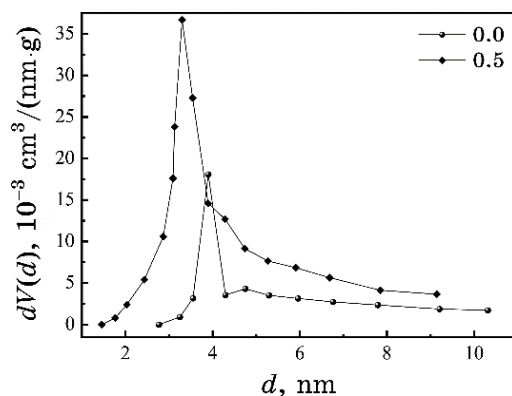


Fig. 6. Nanopores' size distribution for $NiY_xFe_{2-x}O_4$ powders.

3.6. Adsorptive Properties

At present, the study of the adsorption properties of magnetic spinel nanomaterials in relation to a variety of synthetic organic dyes is enough actual. Adsorption studies are aimed at determining the adsorption capacity of the adsorbent (spinel nanomaterial), pH influence, mixing time, output concentration of dye on the adsorption process, data analysis of adsorption isotherms, and include kinetic and thermodynamic calculations.

Adsorption capacity q_{ads} (mg/g) is calculated by the formula:

$$q_{ads} = \frac{(C_0 - C_{eq})V}{m}, \quad (2)$$

where q_{ads} is the adsorption capacity, in mg of dye per 1 gram of dry adsorbent (mg/g); C_0 —initial concentration of dye in solution (mg/l), C_{eq} —final or equilibrium concentration dye in solution (mg/l); V —volume of the investigated solution (l), m —mass of adsorbent (g).

The efficiency of synthesized spinel nanoparticles as adsorbents for removal of various organic dyes from solutions was investigated. Adsorption studies of methylene blue and Congo red dyes were performed at pH = 7 and at temperature $T = 20^\circ\text{C}$. The results of the adsorption studies are presented in Table 3.

The $\text{NiY}_{0.5}\text{Fe}_{1.5}\text{O}_4$ has the highest adsorption capacity among the above spinel ferrites, in particular, it is by 1.84 (for methylene blue) and 2.35 (for Congo red) times greater than that of NiFe_2O_4 . This is explained by the decrease in the particle size, on the one hand, and the partial inversion of the structure that is the location of bipartite cations in the A and B positions of the spinel lattice, on the other hand. Thus, the distribution of cations in the spinel ferrites can be one of the important factors influencing their adsorption capacity.

The influence of the initial concentration of dyes on the adsorption capacity of Ni–Y ferrites was investigated. The increase in the

Table 3. The adsorption capacity of magnetic spinel nanosorbents.

x	Dye 1	q_{ads} , mg/g	Dye 2	q_{ads} , mg/g
0.0		131.2		96.8
0.1		142.1		123.5
0.2	methylene blue	162.4	Congo red	156.3
0.3		190.7		189.7
0.4		225.9		216.3
0.5		240.8		227.2

initial concentration of dyes by 3 times (from 50 to 150 mg/l) results an increase in the adsorption capacity of the ferrite nanopowders by 40%. For example, for $\text{NiY}_{0.3}\text{Fe}_{1.7}\text{O}_4$ sample, adsorption capacity increases from 189.7 mg/g to 265.6 mg/g.

Thus, the adsorption process is very much dependent on the initial concentration of the solution. It is important a simple and fast separation of adsorbed dyes from nanoferrite spinel that can be achieved by the action of an external magnetic field.

4. CONCLUSION

The $\text{NiY}_x\text{Fe}_{2-x}\text{O}_4$ ferrites were synthesized by the SGA technology. Except NiFe_2O_4 , the samples were non-phase and contain additional of $\alpha\text{-Fe}_2\text{O}_3$ and Y_2O_3 phases. The size of powders was found to be in the range of 17 nm to 43 nm. The addition of Y^{3+} ions contributes to the more uniform and causes to decrease particle size. The room temperature infrared spectra of yttrium-substituted nickel ferrite confirm the presence of cubic spinel ferrite phase. All the doping samples clearly show the ferrite formation at 560 cm^{-1} .

Thus, Ni–Y ferrite nanomaterials are promising adsorbents for the removal of organic dyes from sewage. These materials have high chemical resistance, thermal stability and durability, and, consequently, longer lifetimes, unlike traditional adsorbents. The study of adsorption kinetics indicates that the mechanism of adsorption depends on the nature of the adsorbate and adsorbent. It can be concluded that on the adsorption capacity of spinel ferrites affects the distribution of cations between the *A* and *B* positions, the pH value of the solution, and the initial concentration of the organic dye.

REFERENCES

1. G. Kochetov, D. Zorya, and J. Grinenko, *Civil and Environmental Engineering*, **1**, No. 4: 301 (2010); <https://doi.org/10.15587/2312-8372.2018.152615>.
2. B. J. Kahdum, A. J. Lafta, and A. M. Johdh, *Polish Journal of Chemical Technology*, **19**, No. 3: 61 (2017); <https://doi.org/10.1515/pjct-2017-0050>.
3. K. H. Gonawala and M. J. Mehta, *Int. Journal of Engineering Research and Applications*, **4**, No. 5: 102 (2014).
4. V. S. Bushkova and I. P. Yaremiy, *J. Magn. Magn. Mater.*, **461**: 37 (2018); doi.org/10.1016/j.jmmm.2018.04.025.
5. E. J. Mohammad, S. H. Kathim, and A. J. Lafta, *Int. J. Chem. Sci.*, **14**, No. 2: 993 (2016).
6. V. S. Bushkova, *J. Nano- and Electron. Phys.*, **7**: 03021 (2015).
7. A. Rais, A. Addou, M. Ameri, N. Bouhadouza, and A. Merine, *Appl. Phys. A*, **111**: 665 (2013); [doi: 10.1007/s00339-012-7304-9](https://doi.org/10.1007/s00339-012-7304-9).

8. V. S. Bushkova, *Low Temperature Phys.*, **43**: 1724 (2017); <https://doi.org/10.1063/1.5012788>.
9. M. Patange, S. E. Shirsath, S. S. Jadhav, K. S. Lohar, D. R. Mane, K. M. Jadhav, *Mater. Lett.*, **64**: 722 (2010); doi.org/10.1063/1.3559266.
10. O. P. Perez, H. Sasaki, A. Kasuya, B. Jeyadevan, K. Tohji, T. Hihara, K. Sumiyama, *J. Appl. Phys.*, **91**: 6958 (2002); [doi: 10.1063/1.1452193](https://doi.org/10.1063/1.1452193).
11. K. K. Bharathi, G. Markandeyulu, and J. A. Chelvane, *J. Magn. Magn. Mater.*, **321**: 3677 (2009); doi.org/10.1016/j.jmmm.2009.07.011.
12. M. Jacintha, P. Neeraja, M. Sivakumar, and K. Chinnaraj, *J. Supercond. Nov. Magn.*, **30**: 237 (2017); [doi: 10.1007/s40097-017-0248-z](https://doi.org/10.1007/s40097-017-0248-z).
13. V. S. Bushkova and B. K. Ostafiychuk, *Powder Metall. and Metal Ceram.*, **54**: 509 (2016).
14. A. Shaikh, S. Jadhav, S. Watawe, and B. Chongnle, *Mat. Sci. Lett.*, **44**: 192 (2000).
15. W. N. Martens, J. T. Kloprogge, R. L. Frost, and L. Rintoul, *J. of Raman Spectroscopy*, **35**, No. 3: 208 (2004); [doi: 10.1002/jrs.1136](https://doi.org/10.1002/jrs.1136).
16. J. Križan, J. Možina, I. Bajsić, and M. Mazaj, *Acta. Chim. Slov.*, **59**, No. 1: 163 (2012).